DATA REPOSITORY

Paleoseismologic Trenching

We used a standard backhoe to excavate the trenches. Aluminum hydraulic shores were emplaced to ensure trench safety, and the walls were carefully scraped and cleaned to remove any smear created by the backhoe bucket. String lattices were strung on both walls of the northern trench and the southern wall of the southern trench creating grids that were 100 cm (horizontal) by 50 cm (vertical). The trench walls were logged at a scale of 1:15. Locations of sedimentary units, and sediment and tectonic structures were recorded and reported hereinafter according to their trench coordinates, using a horizontal meter measurement staring from the east end of the trenches, and a vertical meter measurement staring from an arbitrary "0" datum. Each grid was logged manually and digitally photographed using a wide-angle camera lens. At a later stage, all photographs were corrected for distortion caused by the camera lens, and also brightness adjustments were made due to lower sun-exposure of the grids at the bottom of the two trenches. All corrected images were finally merged into a photomosaic collage and detailed logs were drafted (Fig. DR3).

Both trenches provide exposure of the main fault zone where units are separated vertically as much as ~0.7 m in the northern trench and ~1.5 m in the southern trench. Evidence for the three most recent events comes from the northern trench, while the oldest event in our study is exposed only in the deeper southern trench. Major stratigraphic units are numbered in increments of 10, increasing with depth, whereas sub-units are labeled using a combination of the respective major stratigraphic unit number plus an alphabetical letter, descending with depth. The oldest unit (unit 100) that we observed is a very-fine-grained, dense green clay that is exposed only at the base of the section to the east of the eastern (main) fault strand. Overlying

this is a 1-m-thick layer, unit 90, composed of coarse-grained sand and gravel that ranges in color from light yellowish-brown to red (locally pale green), and that is locally coated with black manganese oxide. These gravels display both horizontal stratification and prominent cross-stratification, and we interpret the unit to have been deposited in a shallow lacustrine environment. This is the layer with the oldest OSL age that we obtained – 8.4±0.7 ka. Unit 90 is capped by a fine-grained layer which we label as 90A. Above the coarse-grained sands lie well-sorted light greenish-gray sediments. Based on grain size (clay to pebbles), unit 80 can be divided into at least four distinct sub-units (80A, 80B, 80C, and 80D), although the boundaries between them are generally gradational over 5-10 cm. The next-youngest unit is a thick, very pale brown clay layer (unit 70), which is 1 m thick in the northern trench. Unit 70 is one of the thickest layers in the northern trench, but is almost nonexistent in the southern trench. The bottom of this unit yields OSL ages of 6.1±0.4 and 7.3±0.5 ka (two samples dated), whereas the top has OSL ages of 5.4±0.4 and 5.6±0.4 ka (two samples dated). Directly above unit 70 is a darker pinkish-brown layer (unit 60), which is only ~0.15-0.20 thick. It appears to be separated from the paler clay below by flame structures, suggesting liquefaction of water-saturated sediments (probably related to Event 2- see main text for discussion of that surface rupture). On top of this unit is a series of interbedded very pale brown, medium-grained sands, fine-grained sands, and clays (unit 50), roughly 0.75 m thick in the northern trench but only 0.30 cm in the southern trench. This layer consists of at least three subunits labeled 50A, 50B, and 50C. The bottom of unit 50 has an age of 5.6±0.4 ka, whereas the top yields an age of 5.0±0.4 ka (two samples dated). Above this is a carbonate-rich clay layer (unit 40), light brown in color, which we interpret as a cambic soil horizon with an age of 3.4±0.2 ka. Depositionally, unit 40 is part of unit 50. However, we distinguish it as a separate unit based on the development of a carbonate

soil overprinted by a cambic soil. Clays and fine-grained sands lie above unit 40, likely the result of playa deposition in late Holocene time.

On the western side of the fault, the oldest of these layers is a very fine-grained, pinkish-brown clay (unit 30) with distinct upper and lower boundaries. This clay is generally ~0.1 m thick, but it almost doubles in thickness in the footwall of a reverse fault 14 m west of the main strand of the Calico fault. A narrow (~5 cm) lens of very fine-grained sand of the same color is interbedded within this clay layer. One OSL sample was dated from the bottom (2.0±0.1 ka) and two from the top (1.1±0.1 and 0.6±0.1 ka) of unit 30. The clay does not appear on the eastern side of the main fault strand, but a friable, pinkish-brown, very fine-grained sand layer (unit 20) does; this 5-cm-thick fine-grained sand does not exist on the western side of the fault. Both, the clay on the western side and the sand on the eastern side of the fault pinch out within 0.25 m of the main fault. The top-most stratigraphic unit (unit 10) is the most recently deposited playa sediment: a very fine-grained, pinkish-gray silt (~0.3 m). This massive uppermost unit is unbroken by the most recent surface rupture, although it exhibits a substantial (~0.25 m) change in thickness across the fault, thinning to just 5 cm on the east side of the main fault strand.

Optically Stimulated Luminescence Geochronology

The OSL technique relies on the interaction of ionizing radiation with electrons within semi-conducting minerals resulting in the accumulation of charge in metastable location within minerals. Illuminating the minerals and detrapping the charge that combines at luminescence centers can determine the population of this charge. This results in the emission of photons (luminescence). Artificially dosing sub-samples and comparing the luminescence emitted with the natural luminescence can determine the relationship between radiation flux and

luminescence. The equivalent dose (D_E) experienced by the grains during burial therefore can be determined. The other quantity needed to calculate the age is the ionizing radiation dose rate, which can be derived from direct measurements or measured concentrations of radioisotopes. The age is then derived using the equation:

Age = D_E /dose rate

The uncertainty in the age is influenced by the systematic and random errors in the D_E values and the possible temporal changes in the radiation flux. The quoted error is the deviation of the D_E values on multiple sub-samples and the error in measured ionizing radiation dose rate or the concentration of radioisotopes. It is not possible to determine temporal changes in the dose rate that is a consequence of changes in water content and the growth and/or translocation of minerals within the sediment. The dose rate is therefore generally assumed to have remained constant over time.

The collected sediment samples were processed in the Luminescence Dating Laboratory at the University of Cincinnati. The USGS Reactor in Denver for neutron-activation analysis (INAA) was utilized to determine the concentration of radioisotopes for dose-rate determination.

An uncertainty of 10% was applied to each of the determined radioisotope concentrations to account possible micro-variation in concentration within the sediment sample. The total in situ dose-rate from beta and gamma was determined by converting elemental concentrations to beta and gamma dose-rates from Adamiec and Aitken (1998) and applying the Beta attenuation factors for U, Th and K compositions incorporating grain size factors from Mejdahl (1979). Beta attenuation factor for Rb was taken as 0.75 (Adamiec and Aitken, 1998). Variable water content throughout the section may have occurred throughout the history of the section. However, it is not possible to determine the degree of such changes. The dose rate was therefore assumed to

have remained constant and a 10 ± 5% water content value was used to help account for possible changes in water content. The dose-rate from cosmic rays was calculated according to Prescott and Hutton (1994) and an uncertainty of ±10% is applied to account for possible temporal changes. A summary of OSL dating results radioisotopes concentrations, dose-rates, D_E estimates and optical ages are provided in Table 1. The radioisotope concentrations are within the normal range for naturally occurring sediments with dose rates ranging from ~2.8 to 4.3 Gy/ka.

The remaining sediment in the center of the tube was dried in an oven at 50°C. Particle-size fractions 90-125 µm, 125-180 µm, 180-250 µm, 250-500 µm, 500-1000 µm and >1000 µm were obtained by dry-sieving the sediment. The carbonates and organic matter were removed from the dominant fine-grained fraction (90-125 µm/125-180 µm/180-250 µm) using 10% HCl and 30% H_2O_2, respectively. The samples were then treated with 10% HF for 20 minutes to dissolve fine feldspar, followed by 10% HCl for 2 hours to remove any fluorides. Lithium polytungstate solutions of different densities were used to separate the quartz and feldspar-rich fractions from the heavy minerals. The separated quartz-rich fraction was treated with 49% HF for 40-80 min to dissolve any plagioclase feldspars and remove the alpha-irradiated surface of the quartz grains. Dried quartz grains were mounted on stainless steel discs with silicon spray. All the preparation techniques were carried out under laboratory safelights to avoid optical bleaching of the luminescence signal.

Luminescence measurements were undertaken on quartz for the dominant particle size for each sample using a Riso Automated TL/IRSL/Blue DA-15 C/D OSL Dating System. Luminescence from the quartz grains was stimulated using an array of blue light emitting diodes (470 nm, 50 mW/cm^2) filtered using a green long-pass GG-420 filter. Detection was through a

Hoya U-340 filter. All quartz aliquots were screened for feldspar contamination using infrared stimulation with infrared light emitting diodes (870 nm, 150 mW/cm^2). All OSL signals were detected using a 52 mm diameter photomultiplier tube (9235B). Riso Sequence Editor software was used for hardware control.

Equivalent dose (D_E) measurements were determined on multiple aliquots for each sample using the single aliquot regenerative (SAR) method protocol developed by Murray and Wintle (2000). The D_E value for every aliquot of each sample was examined using Riso Analysis 3.22b software. Preheat plateau tests were undertaken on samples 081507D and 081507G to determine a preheated temperature of 240^{o}C. Dose recovery tests were performed on each sample. Aliquots with poor recuperation (>10%) were not used in the age calculations. In fluvial and colluvial sediments partial bleaching of sediment is a problem, and this is reflected in a large spread of D_E values and results in an overestimate of the age. The weighted average of the D_E values and its uncertainty were therefore used in the final age calculation to help account for this issue. The weighted average of the D_E values distribution skews the average D_E value the towards the younger end of the range since the associated errors for older aliquots are greater, while at the same time all the D_E data is included in the calculation. The resultant age and its error, therefore, provide the best representation of all the systematic and random errors. However, the OSL age likely represents the maximum age for the deposition of the sediment.

DATA REPOSITORY FIGURES

Figure DR1: Detailed photo logs between meters 8-12 and meters 21-26 from the northern (reversed) wall of the northern trench. (A) Detailed photo log of the main (eastern) fault strand (between meters 8 and 9). Vertical separation of ~1 m with younger units, 30-50, buttressing

against the scarp of unit 70 plus a fissure fill originating within unit 70, provide evidence for event horizon 3. Upward rupture terminations between meter 10 and meter 12 provide evidence for the most recent event. (B) Detailed photo log between meters 21 and meters 26. The upward rupture terminations can be related to the penultimate event, however it is difficult to discern their upward extent, and thus can be due to the most recent surface rupture.

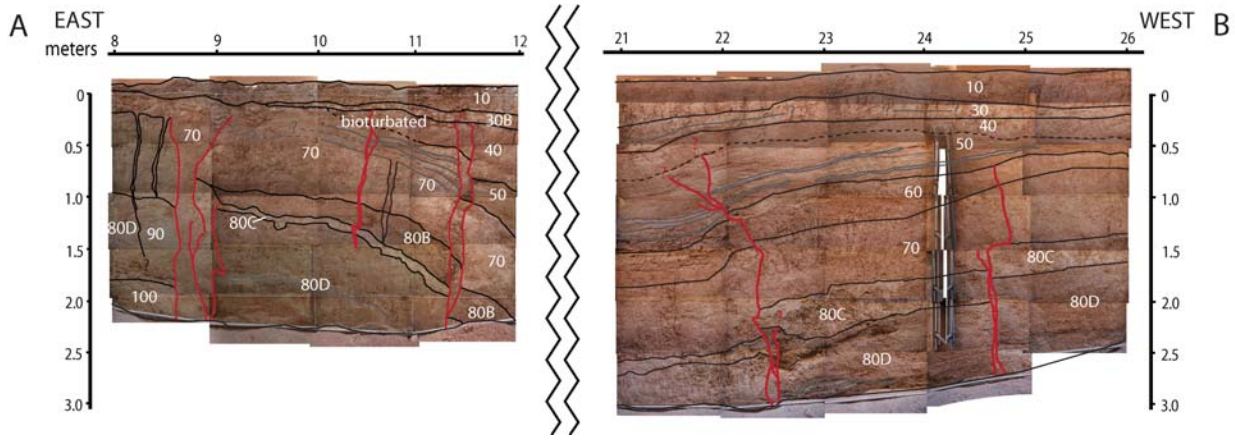

Figure DR2: Evidence of three event horizons (A-C) comes from our northern trench, and evidence of the oldest event horizon (D) comes from our southern trench. (A) Geometry of stratigraphic growth and upward rupture terminations provide evidence in support of the most recent surface rupture. (B) Geometry of stratigraphic growth of unit 50 and possible upward rupture termination within the same unit at meter 25 provide evidence in support of the penultimate event. (C) Vertical separation of ~1 m and fissure fills at the bottom of unit 70 provide evidence in support of the anti-penultimate event. (D) Vertical separation of at least 1.5 m in our southern trench provides evidence in support of the oldest event horizon.

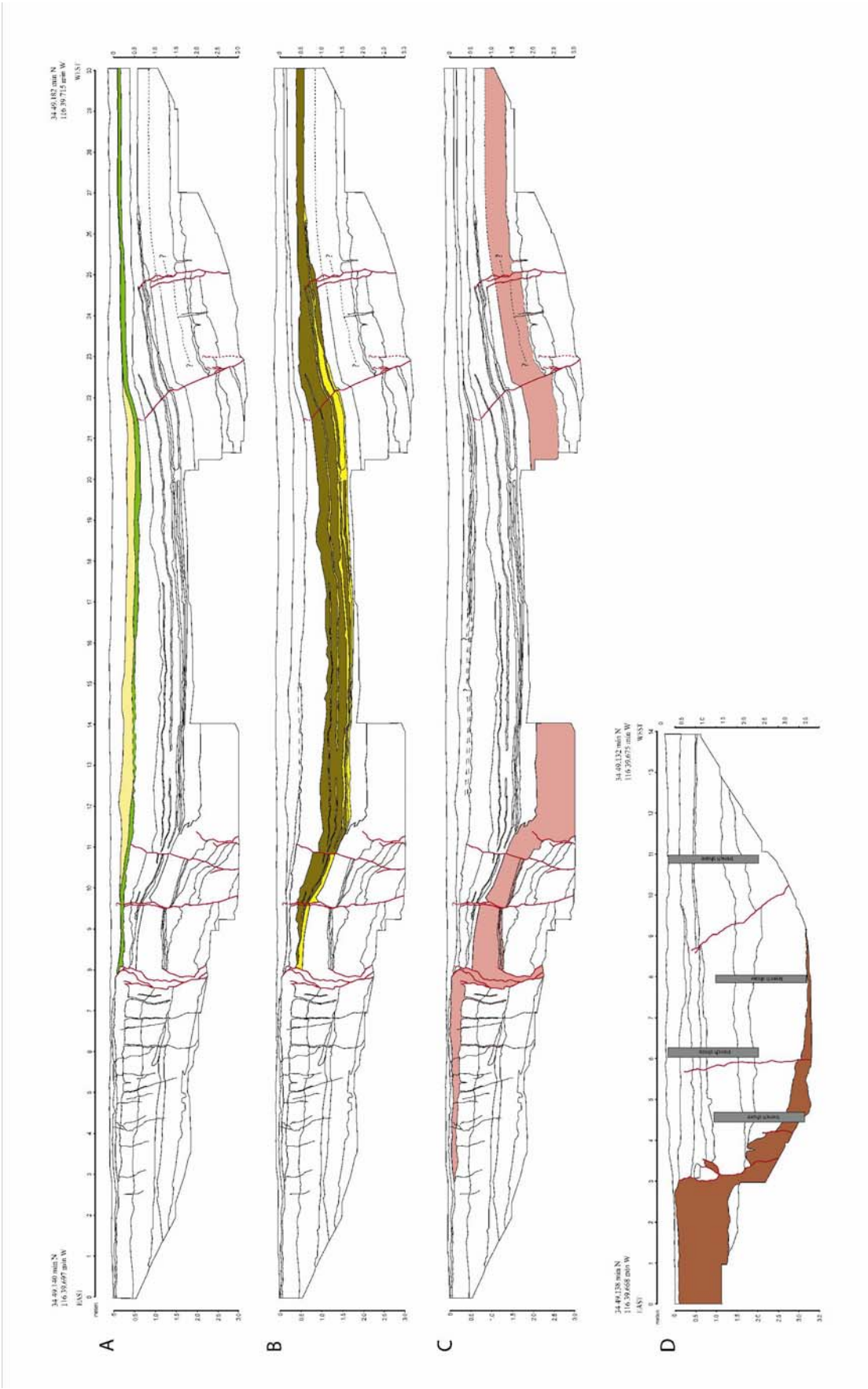
A
B
C
D

Figure DR3: Photomosaic of (A) southern wall and (B) northern wall of the northern trench, and (C) southern wall of the southern trench. The potential of trench collapse prevented us from photologging the northern wall of the southern trench.

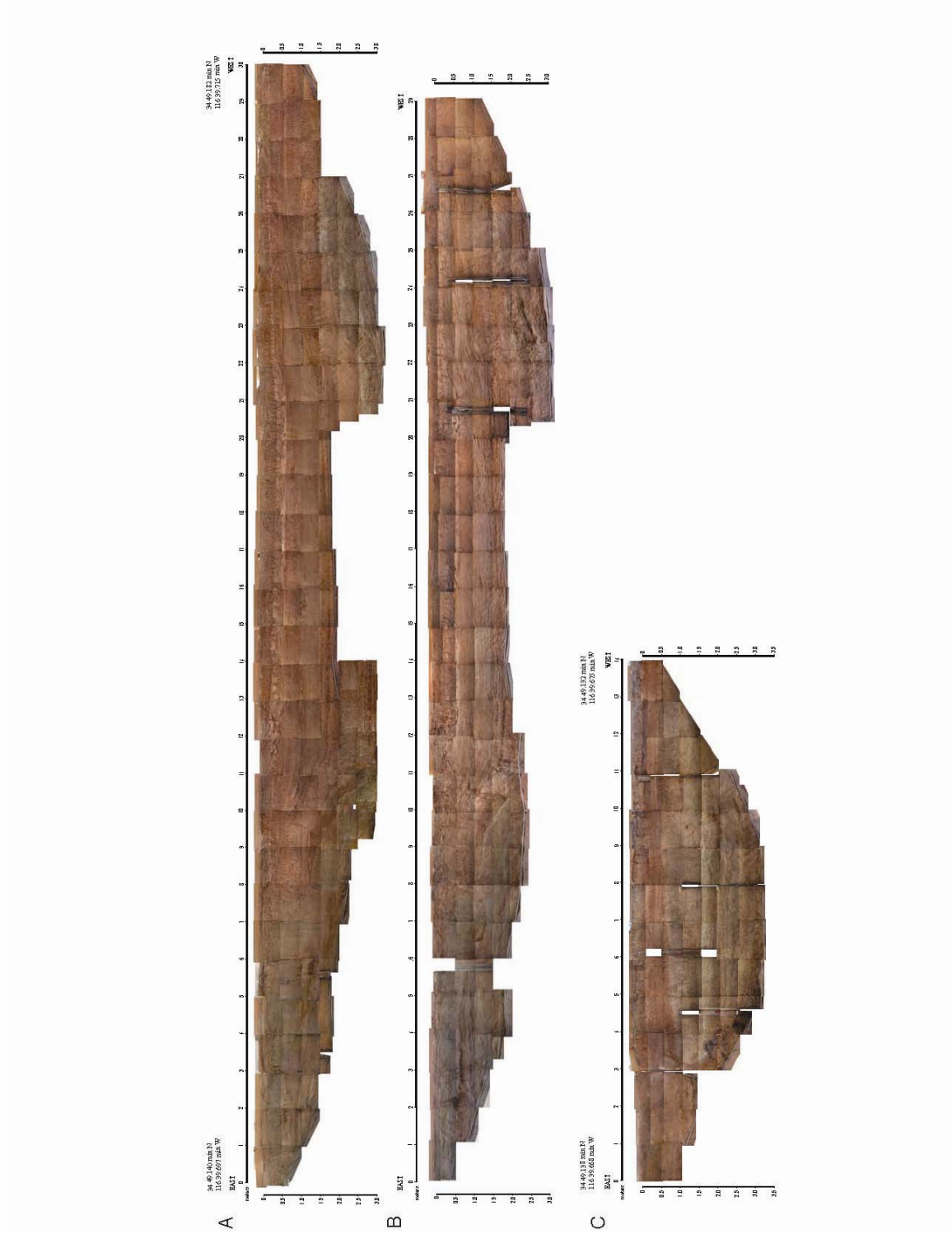
A
B
C